Available online at www.sciencedirect.com
ScienceDirect
LITHOS
Lithos 96 (2007) 90–107
www.elsevier.com/locate/lithos

Petrology and geochronology of Xuejiashiliang igneous complex and their genetic link to the lithospheric thinning during the Yanshanian orogenesis in eastern China

Shangguo Su [a,b,*], Yaoling Niu [c,a,b], Jinfu Deng [a,b], Cui Liu [a,b], Guochun Zhao [a,b], Xingguo Zhao [a,b]

[a] *State Key Laboratory of Geological Processes and Mineral Resources, China University of Geosciences, Beijing 100083, China*
[b] *Key Laboratory of Lithosphere Tectonics and Lithoprobing Technology of Ministry of Education, China University of Geosciences, Beijing 100083, China*
[c] *Department of Earth Sciences, Durham University, Durham DH1 3LE, UK*

Received 22 February 2006; accepted 5 September 2006
Available online 12 January 2007

Abstract

The Xuejiashiliang igneous complex, ~150 km north of the City of Beijing, is an important member of the Mesozoic Yanshanian orogen in eastern China. This complex consists of gabbro, monzogabbro, monzonite, syenite and granite. In situ zircon U/Pb dating shows that the Xuejiashiliang complex was emplaced at ~128.8–123.7 Ma (i.e., K_1^1). Field and petrographic observations together with bulk-rock major element, trace element and Sr–Nd–Pb isotopic data suggest that the gabbro represent remnants of a mafic intrusion formed from cooling of a mantle derived melt that underplated beneath or intruded into the lower crust. The monzogabbro may be the product of deep crustal assimilation of this mantle derived melt. The syenite may have precipitated from a melt produced by deep crustal melting caused by the mantle derived melt. The monzonite may have formed from mixing between melts parental to the syenite and monzogabbro. That is, all these diverse lithologies may have resulted from varying degrees of mantle melt induced crustal melting, melt assimilation, differentiation and mixing. The granite is best interpreted as resulting from upper crustal melting and advanced degrees of differentiation. The remarkably similar Nb–Sr–Pb isotopes of all these lithologies (except for $^{87}Sr/^{86}Sr$ of the granite) with an "EM1-like" signature point to a common source they share. This common source could be ancient lithospheric mantle, but we consider the Archean lower crust to be the more likely candidate. The high $^{87}Sr/^{86}Sr$ (0.8955) of the granite resulted from radiogenic ingrowth of ^{87}Sr due to the elevated Rb/Sr ratio (~22.4). The high $[La/Yb]_{CN}$ and Sr/Y ratios of all these lithologies (except the granite) are consistent with magma genes at depths where garnet is a stable phase. This is consistent with the condition of syenite genes that requires pressures equivalent to depths in excess of 50 km. All these constrain that the complex may have formed at the base of the thickened crust, perhaps genetically associated with episodes of compressional tectonics prior to lithosphere thinning. The widespread early Cretaceous (K_1^1) granitoid magmatism in eastern China, including the Xuejiashiliang complex, requires volumetrically significant basaltic magmas underplating at the base of or intruding within the Archean lower crust. Possible eclogitization of these underplated basaltic magmas/rocks at the base of the thickened crust would raise the bulk density of the lithosphere, thus allowing portions of the

* Corresponding author. State Key Laboratory of Geological Processes and Mineral Resources, China University of Geosciences, Beijing, 100083, China. Tel.: +86 10 82321191; fax: +86 10 82322094.
E-mail address: susg@cugb.edu.cn (S. Su).

0024-4937/$ - see front matter
doi:10.1016/j.lithos.2006.09.020

lithosphere to sink into the asthenosphere. If eclogite foundering is indeed an immediate cause of the lithosphere thinning, then it is critical to understand the origin of volumetrically significant basaltic magmatism beneath eastern China in the Mesozoic for a better understanding of the Yanshanian orogenesis.

Keywords: Petrology and geochronology; Xuejiashiliang igneous complex; Yanshanian orogenesis; Lithospheric thinning

1. Introduction

The cause of the Mesozoic lithosphere thinning in eastern China is highly debated in the solid Earth Science community (see Niu et al., 2005a). There are two prevailing models. One model emphasizes basal erosion, either thermally (Lu et al., 2000; Xu, 2001; Zheng et al., 2003) or by hydration-weakening (Niu, 2005a; Niu et al., 2005b), that transforms basal portions of the lithosphere into asthenosphere. The other model, commonly referred to as delamination, stresses density increase within the lithosphere that triggers its basal portions (Deng et al., 1994; Wu et al., 2002) or even the crust (Gao et al., 2004) to sink into the asthenosphere.

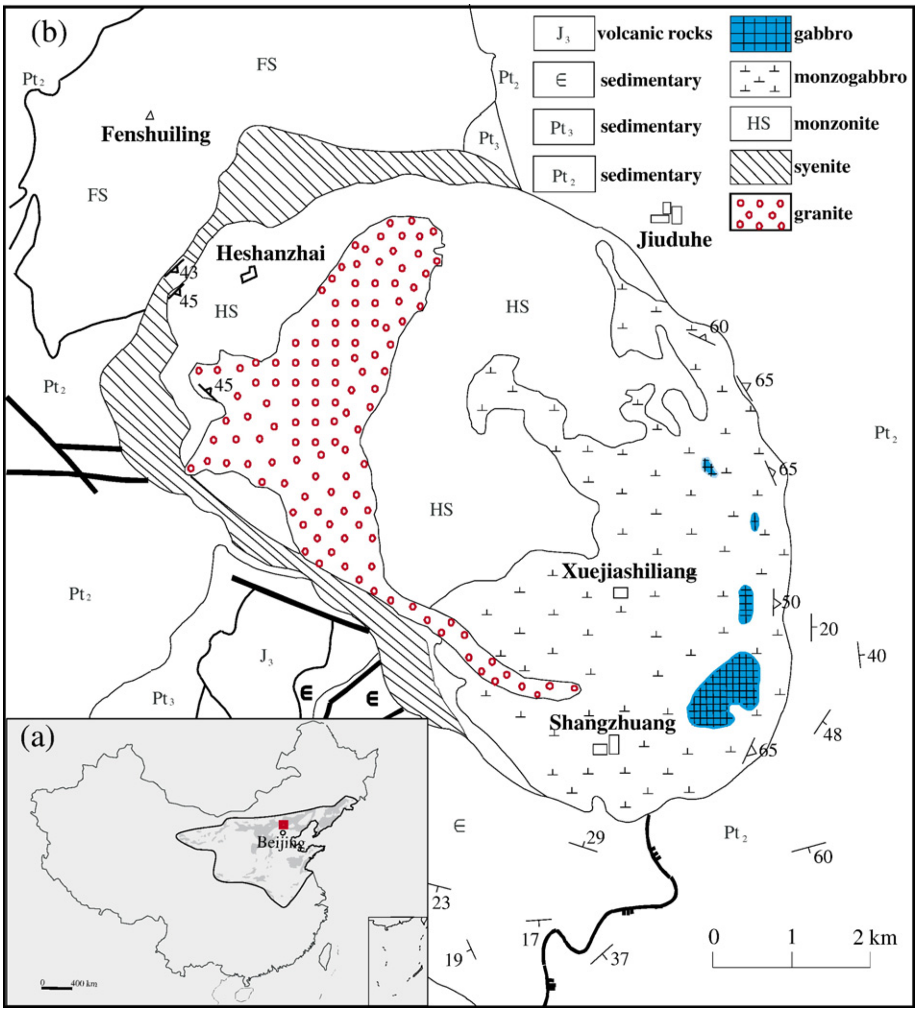

Fig. 1. (a) Showing the location of the studied area, the red square north of Beijing. The triangular region highlights the traditionally defined North China Craton (NCC); (b) details of the geological map of the Xuejiashiliang igneous complex (modified after Yu et al., 1994). (For interpretation of the references to colour in this figure legend, the reader is referred to the web version of this article.)

Table 1
Major and trace element compositions of representative samples of the Xuejiashiliang complex

Sample	WY-2	WY-3	WY-4	WY-14	WY-16	BB1	BB2	BB5	BB6	BB9
	Gabbro	Monzogabbro	Syenite	Granite	Monzonite	Gabbro	Gabbro	Monzogabbro	Syenite	Granite
SiO_2	47.49	45.19	59.26	74.60	54.79	48.49	46.51	57.42	65.96	75.32
TiO_2	1.51	3.00	0.88	0.09	1.59	2.54	2.39	1.41	0.42	0.15
Al_2O_3	16.60	15.92	19.32	14.10	16.94	17.85	16.57	16.75	16.15	13.35
TFe_2O_3	12.20	13.64	4.56	1.09	8.77	10.78	12.35	7.36	3.23	1.11
MnO	0.11	0.17	0.06	0.02	0.13	0.14	0.13	0.10	0.09	0.06
MgO	7.60	5.21	1.44	0.01	3.06	4.29	5.61	3.17	0.45	0.17
CaO	10.53	8.83	3.67	0.24	5.66	8.33	8.05	4.67	1.66	0.57
Na_2O	2.97	3.98	5.31	5.08	5.38	4.59	4.09	4.82	5.38	4.54
K_2O	0.61	1.64	4.35	4.42	3.14	1.40	1.88	3.14	5.78	4.79
P_2O_5	0.20	1.75	0.42	0.01	0.59	1.05	1.38	0.59	0.10	0.02
LOI	0.92	1.12	0.53	0.21	0.77	0.39	0.68	0.42	0.40	0.39
TOTAL	99.93	99.62	99.54	99.85	100.28	99.85	99.64	99.85	99.62	100.47
Trace elements (ppm)										
Ba	474.0	1250.0	4098.0	16.5	1667.0	1199.0	1763.0	1562.0	497.0	38.0
Rb	7.45	28.50	59.00	184.00	43.20	19.00	29.00	77.00	153.00	118.00
Sr	1236.00	1541.00	1348.00	8.21	827.00	1666.00	1875.00	1191.00	104.00	13.00
Cs	0.09	0.41	0.66	0.86	0.48					
Li	5.77	13.50	18.40	29.00	14.00					
Ga	18.60	23.30	22.30	20.20	23.00					
Ta	0.28	1.32	0.98	3.38	1.11	1.39	0.92	1.12	2.78	2.40
Nb	4.92	27.50	18.90	50.80	21.30	28.00	21.00	20.00	51.00	33.00
Hf	1.33	3.31	6.05	7.26	2.97	2.51	2.44	4.45	12.80	4.72
Zr	49.80	136.00	298.00	162.00	127.00	129.00	134.00	231.00	649.00	163.00
Y	9.67	37.10	15.40	7.92	23.50	26.00	25.00	16.00	24.00	14.00
Th	0.46	1.65	3.09	30.90	2.54	1.02	1.09	5.97	17.80	12.90
U	0.13	0.63	0.90	4.61	0.71	0.82	0.55	1.87	4.34	1.97
Cr	218.00	6.63	2.57	21.70	22.20	20.00	54.00	58.00	15.00	22.00
Ni	148.00	7.20	2.72	2.88	17.40	19.00	57.00	30.00	16.00	13.00
Co	53.30	28.30	7.38	0.14	19.90	34.00	44.00	20.00	6.00	5.00
Sc	23.10	20.60	5.00	1.00	13.00	18.30	16.40	8.96	4.45	1.57
V	264.00	205.00	46.60	2.02	138.00	124.00	185.00	75.00	10.00	10.00
Cu	70.10	28.30	10.30	0.94	22.50					
Pb	3.22	8.28	22.80	38.80	18.60					
Zn	83.80	150.00	70.60	41.70	104.00					
REE (ppm)										
La	12.60	83.10	49.90	29.20	55.30	63.30	79.60	70.00	81.90	79.70
Ce	27.50	150.00	89.40	52.20	107.00	116.00	155.00	122.00	138.00	118.00
Pr	3.26	20.00	9.10	3.73	11.50					
Nd	14.60	84.60	34.90	9.38	46.10	58.90	77.30	56.50	48.60	35.80
Sm	3.17	15.30	5.80	1.13	8.34	10.90	12.20	8.45	7.87	4.81
Eu	1.14	3.94	3.62	0.08	2.60	3.44	3.79	2.50	1.06	0.46
Gd	2.90	13.00	5.14	1.31	7.36					
Tb	0.36	1.50	0.58	0.15	0.87	1.12	1.12	0.70	0.77	0.45
Dy	1.87	7.21	2.82	0.91	4.46					
Ho	0.37	1.34	0.54	0.23	0.85					
Er	0.87	3.20	1.38	0.79	2.12					
Tm	0.11	0.42	0.20	0.16	0.29					
Yb	0.69	2.42	1.18	1.30	1.76	2.26	2.07	1.32	2.80	1.69
Lu	0.11	0.36	0.19	0.23	0.25	0.37	0.25	0.16	0.42	0.24

BB1, BB2, BB5, BB6, BB9 are from Wang and Zhang (2001).

If the lithosphere thinning is caused by basal erosion (whether thermally or by hydration-weakening), then the genetically associated magmatism would have geochemical signatures of ancient metasomatized lithospheric mantle (being transformed into the asthenosphere). That is, the mantle source component would be

Table 2
Sr–Nd–Pb isotopic data of representative samples of the Xuejiashiliang complex

Sample	Name	$^{87}Sr/^{86}Sr$	$^{143}Nd/^{144}Nd$	$\varepsilon_{Nd}(t)$	$^{206}Pb/^{204}Pb$	$^{207}Pb/^{204}Pb$	$^{208}Pb/^{204}Pb$
WY-2	Gabbro	0.705383	0.512057	−7.3	16.4406	15.2278	36.3936
WY-3	Monzogabbro	0.705388	0.512099	−6.5	16.4339	15.1817	36.2270
WY-4	Syenite	0.705590	0.512025	−7.9	16.4785	15.2064	36.3436
WY-14	Granite	0.895478	0.511851	−11.3	16.1368	15.1134	35.9565
WY-16	Monzonite	0.705663	0.512047	−7.5	16.4069	15.1965	36.2726

geochemically enriched in terms of incompatible elements and radiogenic isotopes. On the other hand, if the lithosphere thinning resulted from basal delamination, then the mantle source component would have geochemically depleted signatures of the upwelling asthenosphere. Of course, crustal level assimilation/contamination may obscure these otherwise distinct signatures.

In this paper, were report new petrologic, geochemical and geochronological data together with field observations on the Xuejiashiliang plutonic complex, which is ~150 km north of the City of Beijing (Fig. 1) and has a total outcrop area of ~30 km^2. This complex is important because it contains the most mafic or least evolved mantle derived rocks in the entire Yanshan orogenic belt, and because it is a self-contained system with a variety of lithologies including gabbro, monzogabbro, monzonite, syenite and granite (Fig. 1), whose detailed investigations hold promise for a better understanding of the Yanshanian orogenesis and for providing useful constraints on the timing and cause of lithosphere thinning during the Mesozoic in eastern China.

2. The Xuejiashiliang igneous complex and brief petrography

Fig. 1 shows the lithological distribution within the complex. From southeast to northwest a regabbro, monzogabbro, monzonite, and granite. Syenite occurs mostly along northern and western margins of the complex (Fig. 1).

Gabbro occurs as small lenses or pods towards the southeastern margin of the complex. It is massive, mostly fresh, and has typical gabbroic textures. It consists of plagioclase (~50 vol.% with $An_{48.3}$), augite (~25 vol.%, $En_{41.2}Fs_{15.2}Wo_{43.6}$), hypersthene (~5 vol.%, $En_{77.5}Fs_{22.5}$), magnesian amphibole (~10 vol.%), magnesian biotite (~5 vol.%), titanomagnetite (~2 vol.%) and minor olivine in some samples.

Monzogabbro occupies much of the southern part of the complex. The major minerals are plagioclase (~55 vol.%, $An_{27.6}$), augite (~20 vol.%), amphibolite (~10 vol.%), biotite (~10 vol.%), rapakivi feldspars (~5 vol.%) and minor amounts of magnetite and quartz.

Table 3
SHRIMP geochronology data of zircons from the Xuejiashiliang gabbro

Spot	$^{206}Pb_c$ (%)	U ppm	Th ppm	Th/U	$^{206}Pb^*/^{238}U$ Age(204c)	1σ err	$^{206}Pb^*/^{238}U$ Age(207c)	1σ err	$^{206}Pb^*/^{238}U$ Age(208c)	1σ err	Total $^{238}U/^{206}Pb^*$	% err	Total $^{207}Pb^*/^{206}Pb^*$	% err
WY-2-1.1	1.76	636	410	0.67	126.1	1.3	127.9	1.2	127.9	1.3	49.72	0.9	.0516	3.0
WY-2-2.1	0.15	2171	746	0.36	393.8	1.1.4	393.8	1.4	393.6	1.5	15.85	0.4	.0557	1.3
WY-2-3.1	7.30	74	90	1.26	124.6	4.9	129.7	3.5	130.0	4.9	47.52	2.6	.0761	7.1
WY-2-3.2	14.17	40	43	1.11	120.4	7.6	133.4	4.9	132.0	6.5	45.52	3.5	.0872	9.1
WY-2-4.1	3.64	184	266	1.49	198.7	3.7	203.3	3.0	204.1	4.2	30.79	1.4	.0610	4.2
WY-2-5.1	1.21	279	481	1.78	202.6	2.4	203.8	2.4	204.6	3.6	30.94	1.1	.0550	3.5
WY-2-6.1	0.17	403	146	0.38	1583.0	9.0	1467.0	9.3	1571.7	10.0	3.59	0.6	.1644	0.6
WY-2-7.1	2.24	527	514	1.01	128.1	2.4	130.5	2.2	129.3	2.6	48.70	1.7	.0521	3.2
WY-2-8.1	2.90	171	147	0.89	125.5	2.4	127.0	2.3	126.6	2.8	49.40	1.7	.0621	5.3
WY-2-9.1	17.75	38	33	0.89	110.1	11.2	127.2	4.8	123.9	6.1	47.76	3.6	.0867	9.6
WY-2-10.1	3.16	123	120	1.01	129.7	4.0	131.9	2.7	130.3	3.4	47.66	2.0	.0607	6.2

Errors (±%) are 1σ; Pb_c and Pb* are common Pb and radiogenic Pb respectively; $^{206}Pb^*/^{238}U$ ages are corrected by common lead and supposed $^{206}Pb^*/^{238}U$–$^{207}Pb^*/^{235}U$ concordia.

Table 4
SHRIMP geochronology data of zircons from the Xuejiashiliang monzogabbro

Spot	$^{206}Pb_c$(%)	U ppm	Th ppm	Th/U	$^{206}Pb^*$ ppm	$^{206}Pb^*/^{238}U$ Age		Total $^{238}U/^{206}Pb^*$	±%	Total $^{207}Pb^*/^{206}Pb^*$	±%
WY-3-1.1	3.69	176	199	1.17	3.14	130.6	±3.4	48.2	2.6	0.0596	5.1
WY-3-2.1	1.17	350	294	0.87	6.49	137.0	±3.2	46.4	2.3	0.0515	3.9
WY-3-3.1	2.23	372	307	0.85	6.68	131.8	±3.0	47.9	2.3	0.0574	3.7
WY-3-4.1	1.84	470	260	0.57	8.33	131.5	±3.3	48.4	2.5	0.0507	3.6
WY-3-5.1	1.74	413	184	0.46	7.60	135.6	±3.1	46.7	2.3	0.0551	3.6
WY-3-6.1	3.75	217	80	0.38	3.82	130.3	±3.3	48.7	2.5	0.0530	5.2
WY-3-7.1	1.11	229	87	0.39	4.07	130.4	±2.0	48.47	1.5	0.0565	4.8
WY-3-8.1	–	145	141	1.00	2.60	132.4	±2.5	47.89	1.8	0.0538	6.0
WY-3-9.1	1.23	172	184	1.11	3.06	131.0	±2.3	48.31	1.7	0.0550	5.5
WY-3-10.1	9.44	133	93	0.73	2.40	132.0	±2.6	47.66	1.9	0.0596	6.0
WY-3-11.1	0.37	711	587	0.85	12.4	129.1	±1.1	49.25	0.86	0.0515	3.6
WY-3-12.1	0.90	159	154	1.01	2.88	133.8	±2.8	47.28	2.0	0.0555	5.9

Errors (±%) are 1σ; Pb_c and Pb* are common Pb and radiogenic Pb respectively; $^{206}Pb^*/^{238}U$ ages corrected by common lead and supposed $^{206}Pb^*/^{238}U$–$^{207}Pb^*/^{235}U$ age concordia.

Monzonite crops out in much of the central and northern portions of the complex. Its mineralogy includes plagioclase (~45 vol.%, An_{22}), alkali-feldspar (~55 vol.%, $Or_{87}Ab_{13}$), biotite (~9 vol.%), amphibole (~7 vol.%), and quartz (~4 vol.%). The monzonite body shows weak schistosity (strike 94° and dip 37°S), and contains some mafic micro-granular enclaves. In a drill hole in the Xihu village, monzonite grades down hole to syenite and the mafic enclaves increase in abundance. The drill core then changes back to monzonite at ~50 m depth.

Syenite occurs along the northern and western margins of the complex. It shows locally well developed schistosity (strike 40° and dip 65°E), and consists of alkali-feldspar (~75 vol.%, $Or_{97\text{-}98}Ab_{2-3}$), plagioclase (~10 vol.%, An_{20}), biotite (~6 vol.%), amphibole (~vol. 5%), and quartz (~4 vol.%).

Granite is mainly located in the central part of the complex. Its major constituent minerals are quartz (~30 vol.%), plagioclase (~30 vol.%, An_{10}) and alkali-feldspar (~35 vol.%, $Or_{96}Ab_4$) plus accessory biotite, amphibole and magnetite.

3. Analytical techniques

Representative samples were analyzed for bulk-rock major elements, trace elements and Sr–Nd–Pb isotopic ratios. Samples were carefully crushed and powdered in agate mortars. Major and trace element data were collected in the Key Laboratory of Continental Dynamics, Northwest University of China. Major element oxides were analyzed using a Rikagu RIX 2100 X-ray fluorescence (XRF) spectrometer on fused glass disks (Gao et al., 2002).

Table 5
SHRIMP geochronology data of zircons from the Xuejiashiliang monzonite

Spot	$^{206}Pb_c$(%)	U ppm	Th ppm	Th/U	$^{206}Pb^*$ ppm	$^{206}Pb^*/^{238}U$ Age		Total $^{238}U/^{206}Pb^*$	±%	Total $^{207}Pb^*/^{206}Pb^*$	±%
WY-16-1.1	1.14	125	133	1.10	2.21	129.7	±2.7	48.64	2.0	0.0577	6.2
WY-16-2.1	2.77	78	68	0.90	1.35	124.5	±3.3	49.9	2.6	0.0706	7.5
WY-16-3.1	2.40	85	79	0.96	1.47	125.6	±3.1	49.6	2.4	0.0677	7.2
WY-16-4.1	3.19	78	73	0.96	1.32	121.5	±3.3	50.9	2.6	0.0738	7.3
WY-16-5.1	0.75	244	229	0.97	4.09	123.6	±1.8	51.29	1.5	0.0545	4.8
WY-16-6.1	3.01	80	72	0.94	1.43	129.8	±3.4	47.7	2.5	0.0726	7.1
WY-16-7.1	2.52	95	77	0.84	1.65	125.8	±3.0	49.5	2.3	0.0686	6.8
WY-16-8.1	0.98	101	91	0.94	1.76	129.0	±2.9	49.0	2.2	0.0564	6.8
WY-16-9.1	0.81	185	157	0.88	3.19	127.0	±2.4	49.85	1.9	0.0550	5.4
WY-16-10.1	2.32	84	76	0.93	1.46	125.8	±3.2	49.5	2.5	0.0670	7.2
WY-16-11.1	1.83	117	104	0.92	1.99	124.1	±2.7	50.5	2.1	0.0631	6.3
WY-16-12.1	1.20	201	176	0.90	3.29	120.5	±2.1	52.38	1.6	0.0580	8.5

Errors (±%) are 1σ; Pb_c and Pb* are common Pb and radiogenic Pb respectively; $^{206}Pb^*/^{238}U$ ages corrected by common lead and supposed $^{206}Pb^*/^{238}U$–$^{207}Pb^*/^{235}U$ age concordia.

Table 6
SHRIMP geochronology data of zircons from the Xuejiashiliang syenite

Spot	$^{206}Pb_c$ %	U ppm	Th ppm	Th/U	$^{206}Pb^*/^{238}U$ Age (204)	1σ err	$^{206}Pb^*/^{238}U$ Age (208)	1σ err	$^{206}Pb^*/^{238}U$ Age (207)	1σ err	Total 238/206	% err	Total 207/206	% err
WY-4-1.1	7.31	94	65	0.71	118.4	3.7	124.7	2.9	124.9	3.4	49.98	2.3	.0675	6.7
WY-4-2.1	2.43	144	153	1.10	123.8	2.7	126.0	2.5	123.0	3.2	50.32	1.9	.0541	6.3
WY-4-3.1	2.86	303	372	1.27	120.2	2.1	122.7	1.7	123.0	2.2	51.60	1.4	.0553	4.3
WY-4-4.1	3.25	126	175	1.43	125.2	3.1	128.3	2.6	127.8	3.7	49.34	2.0	.0549	6.4
WY-4-5.1	0.70	110	123	1.16	123.6	3.6	122.7	2.8	121.9	3.6	51.28	2.2	.0602	7.1
WY-4-6.1	2.38	226	111	0.51	125.6	2.1	127.4	1.9	127.3	2.1	49.60	1.5	.0567	4.7
WY-4-7.1	16.55	59	65	1.15	101.4	7.2	116.8	3.6	115.8	4.9	52.62	3.0	.0784	8.0
WY-4-8.1	4.76	86	68	0.81	123.8	3.7	125.8	3.0	127.8	3.8	49.11	2.3	.0742	6.5
WY-4-9.1	2.83	133	203	1.58	125.8	2.6	127.5	2.5	126.7	3.7	49.31	1.9	.0603	5.9
WY-4-10.1	1.72	145	79	0.56	126.1	2.4	126.9	2.4	125.8	2.7	49.76	1.8	.0572	5.8

Errors (±%) are 1σ; Pb_c and Pb* represent common Pb and radiogenic Pb respectively; $^{206}Pb^*/^{238}U$ ages corrected by common lead, supposed $^{206}Pb^*/^{238}U$–$^{207}Pb^*/^{235}U$ ages concordia.

Trace elements were analyzed using an Elan 6100 DRC Inductively-Coupled Plasma Mass Spectrometer (ICP-MS) on acid digested and diluted solutions following the procedure of Gao et al. (2002). Some of the trace elements were also analyzed by XRF on compressed rock power pellets. Sr, Y, Nb, Zr, Cr and Ni analyses obtained using both methods agree well within 10% uncertainty (Rudnick et al., 2004). Analyses of the United States Geological Survey (USGS) rock standards (BCR-2, BHVO-1 and AGV-1) indicate precisions and accuracies better than 5% for major elements and 10% for trace elements. The analytical data are given in Table 1.

Sr, Nd and Pb isotopic analyses were done in the Isotopic Laboratory of the Chinese Academy of Geological Sciences, Beijing, using a VG354 mass spectrometer following the sample preparation and analytical procedures of Wu et al. (2005a) and Wu et al. (2005b). International reference materials were analyzed along with the unknowns. Repeated analyses gave $^{87}Sr/^{86}Sr = 1.20055 \pm 2$ (NBS607), $^{143}Nd/^{144}Nd = 0.511855 \pm 9$ (La Jolla), $^{143}Nd/^{144}Nd = 0.512651 \pm 9$ (BCR-1), and $^{204}Pb/^{206}Pb = 0.05900 \pm 0.0008$, $^{207}Pb/^{206}Pb = 0.91439 \pm 17$ and $^{208}Pb/^{206}Pb = 2.16441 \pm 97$ (NBS981). The analytical data are given in Table 2.

Zircon crystals from all the lithologies of the Xuejiashiliang complex were extracted following traditional methods. Zircon concentrates so obtained were further hand-picked under a binocular microscope before being prepared for in situ U–Pb geochronological study following the procedure of Jian et al. (2003). The analyses were done using the SHRIMP II at Beijing SHRIMP Center following the procedure of Compston et al. (1992) and Williams (1998). Reference zircon standards TEM (417 Ma) and SL13 (572 Ma) (Nutman et al., 2001) were repeatedly analyzed along with the sample zircons. The analytical data are given in Tables 3–7.

Table 7
SHRIMP geochronology data of zircons from the Xuejiashiliang granite

Spot	$^{206}Pb_c$ %	U ppm	Th ppm	Th/U	$^{206}Pb^*/^{238}U$ Age (204corr)	1σ err	$^{206}Pb^*/^{238}U$ Age (207corr)	1σ err	Total $^{238}U/^{206}Pb^*$	% Err	Total $^{207}Pb/^{206}Pb^*$	% Err
WY-14-3.1	9.04	6980	9159	1.36	101.5	0.7	101.5	0.6	57.34	0.4	.1192	2.5
WY-14-3.2	6.58	4140	6855	1.71	122.1	0.8	122.7	0.5	48.88	0.4	.0967	1.0
WY-14-4.1	0.03	5932	7061	1.23	127.2	0.4	127.2	0.4	50.15	0.3	.0493	1.0
WY-14-5.1	0.01	8882	7455	0.87	131.8	0.4	131.8	0.4	48.40	0.3	.0487	0.8
WY-14-6.1	0.23	5587	2020	0.37	127.2	0.4	127.2	0.4	50.06	0.3	.0504	1.1
WY-14-7.1	0.32	8351	17851	2.21	127.0	0.4	127.0	0.4	50.11	0.3	.0509	1.1
WY-14-8.1	0.61	3521	3901	1.14	123.8	0.6	123.6	0.5	51.24	0.4	.0550	1.3
WY-14-9.1	0.15	5019	3865	0.80	124.6	0.5	124.2	0.4	51.17	0.4	.0519	1.1
WY-4-10.1	0.32	5872	7613	1.34	123.8	0.4	123.6	0.4	51.40	0.3	.0527	1.0
WY-14-11.1	1.38	4660	4294	0.95	122.7	0.5	122.6	0.5	51.30	0.4	.0601	1.6

Errors (±%) are 1σ; Pb_c and Pb* are common Pb and radiogenic Pb respectively; $^{206}Pb^*/^{238}U$ ages are corrected by common lead and supposed $^{206}Pb^*/^{238}U$–$^{207}Pb^*/^{235}U$ age concordia.

4. Results

4.1. Zircon SHRIMP ages

Many age data exist on the complex, ranging from ~120 Ma to ~159 Ma obtained using K–Ar and single zircon U–Pb techniques (Bai et al., 1991; Beijing Bureau of Geology, 1991; Bao et al., 2001; Davis et al., 2001).

In this study, zircons in gabbro are divided into two types. Type 1 zircons are pinkish, euhedral, zoned (Fig. 2: 1.1, 3.1, 3.2, 7.1, 8.1, 9.1, 10.1) and have U/Th ≥ 0.67, consistent with them being of magmatic origin. Type 2 zircons are light yellow, anhedral, have cracks and resorbed edges with or without distinct inner cores (Fig. 2: 2.1, 4.1, 5.1, 6.1) and variable U/Th ratios (0.36–1.78). The U/Th ratio in the inner core regions of Type 2 zircons is ~0.38. We infer that type 2 zircons were inherited from old metamorphic rocks. The data are presented in Table 3 and Fig. 3. The $^{206}Pb/^{238}U$ age of six magmatic zircons varies from 120.4 to 129.7 Ma with an average of 128.8 ± 1.7 Ma (Fig. 3b).

Zircons in monzogabbro are light yellow, granular and zoned (Fig. 4). The data are represented in Table 4 and Fig. 5. The $^{206}Pb/^{238}U$ age of twelve zircons varies from 129.1 to 137.0 Ma with an average of 130.0 ± 1.7 Ma (Fig. 5).

Zircons in monzonite are light yellow or pink, euhedral and prismatic with or without resorbed edges (Fig. 6). The data are represented in Table 5 and Fig. 7. The $^{206}Pb/^{238}U$ age of twelve zircons varies from 120.5 to 129.7 Ma with an average of 125.1 ± 1.5 Ma (Fig. 7).

Zircons in syenite are light yellow or white, euhedral and prismatic with simple or complex zoning (Fig. 8). The data are presented in Table 6 and Fig. 9. The $^{206}Pb/^{238}U$ age of eight out of ten zircons varies from 120.2 to 126.1 Ma with an average of 124.2 ± 1.8 Ma (Fig. 9). The younger ages of WY-4–1.1 (118.4 Ma) and WY-4–7.1 (101.4 Ma) may be due to Pb loss.

Zircons in granite are light yellow or pink, euhedral prismatic or granular with abundant cracks and zoning (Fig. 10). The data are presented in Table 7 and Fig. 11. The $^{206}Pb/^{238}U$ age of six zircons is essentially the same within error: 122.1–124.6 Ma with an average of 123.7 ± 1.1 Ma (Fig. 11b). The other three zircons give an age of 127.0–127.8 Ma. Sample WY-14–5.1 gives 131.8 Ma, which may be relict of an old magmatic zircon.

4.2. Major elements

Fig. 12 shows that the chemical classification of representative samples from the Xuejiashiliang complex corresponds well to field and petrographic classifications (see above). They are gabbro, monzogabbro, monzonite, syenite, and granite. These rocks are located mainly on the alkaline fields. On SiO_2 variation diagrams (Fig. 13), the monzogabbro, monzonite and syenite define linear trends, but the gabbro and granite do not. The apparent variation from gabbro to monzogabbro could represent different cumulates resulting from the "basaltic" stage fractional crystallization of the same mafic melts (Fig. 13) although the elevated K_2O in monzogabbro (Fig. 12) would require some sort of

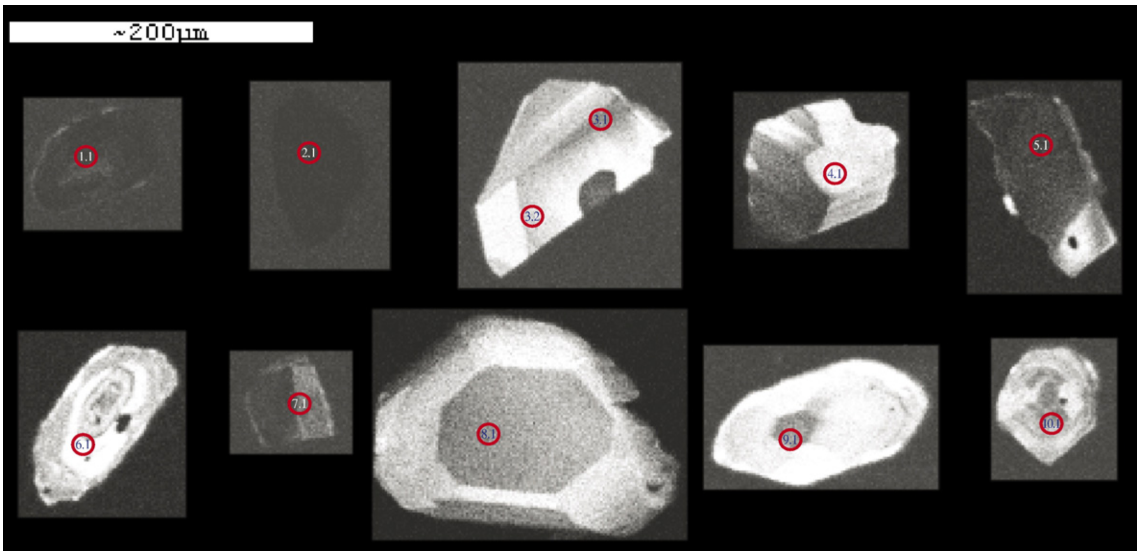

Fig. 2. Cathodoluminescence (CL) images of zircon crystals from gabbro dated by SHRIMP $^{206}Pb/^{238}U$ method at spots circled with labels.

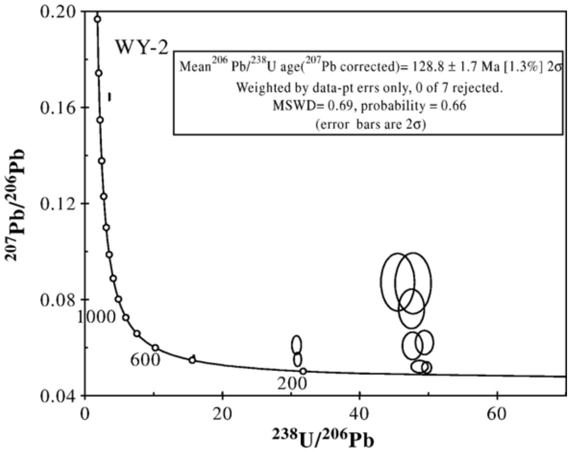

Fig. 3. SHRIMP U–Pb age dates of zircon crystals from gabbro as shown in Fig. 2.

assimilation. The linear trends (Fig. 13) defined by monzogabbro, monzonite and syenite may reflect progressive degrees of differentiation in terms of major elements, but could very well be the results of melt mixing if incompatible trace elements levels are also considered (see Fig. 13).

4.3. Trace elements

Chondrite-normalized rare earth element (REE) patterns (Fig. 14) of the gabbro, monzogabbro, monzonite, and syenite are quite similar with an overall enrichment in light REEs over heavy REEs, giving elevated $(La/Yb)_{CN}$ ratios from 12.3 to 23.2. These rocks have both positive and weak negative Eu anomalies. The syenite has a strong positive Eu anomaly (Eu/Eu* = 1.99), suggesting that plagioclase is not a residual phase in its magma source region, but could be due to excess plagioclase accumulation in the samples. The heavy REE depletion (with respect to light REEs) in igneous rocks is often interpreted as resulting from garnet as a residual phase that holds heavy REEs in the melting region, but garnet could very well be a liquidus phase and its crystallization/removal would have the same effects in the subsequent melts. In either case, the "garnet signature" in these rocks requires the processes to take place at deep levels of a thickened crust (Huang

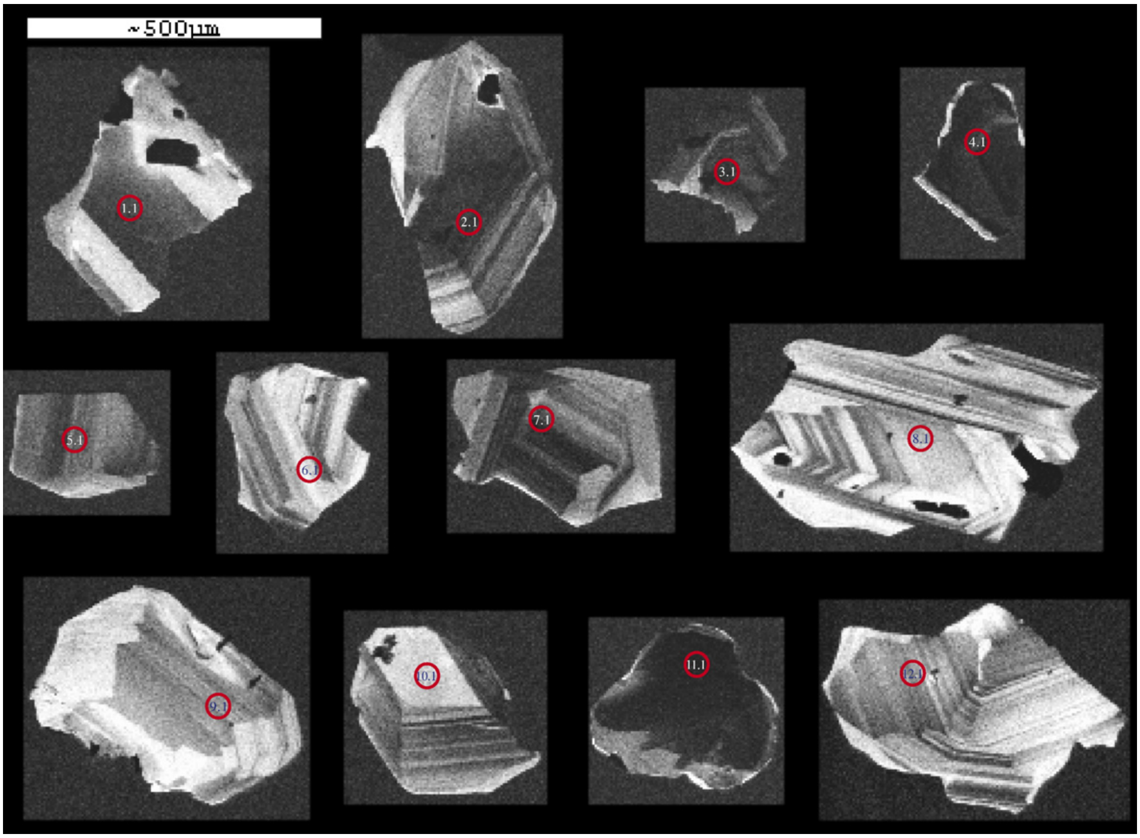

Fig. 4. Cathodoluminescence (CL) images of zircon crystals from monzogabbro dated by SHRIMP $^{206}Pb/^{238}U$ method at spots circled with labels.

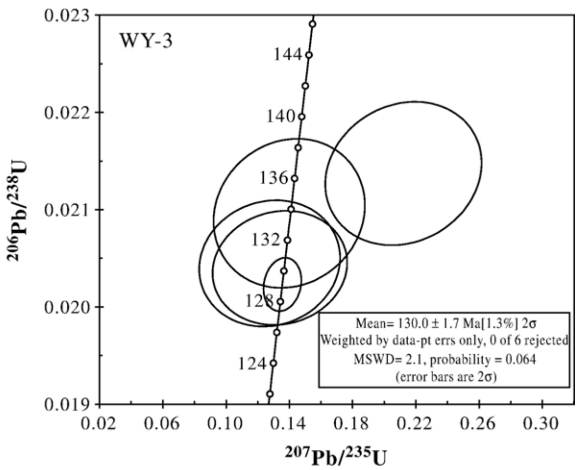

Fig. 5. SHRIMP U–Pb age dates of zircon crystals from monzogabbro as shown in Fig. 4.

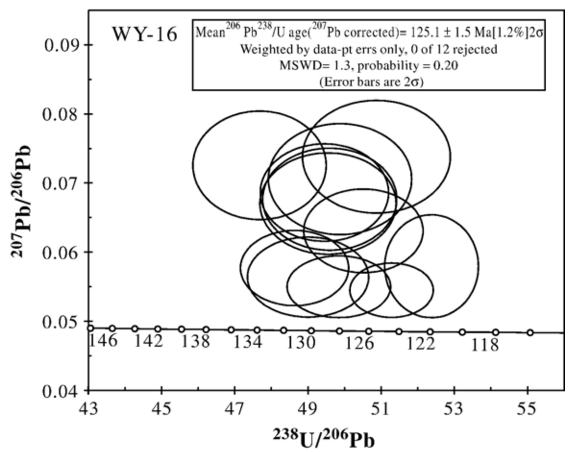

Fig. 7. SHRIMP U–Pb age dates of zircon crystals from monzonite as shown in Fig. 6.

and Wyllie, 1981; Deng et al., 1998). The granite is also enriched in light REEs with elevated $(La/Yb)_{CN}$ ratio of ~15.14, but the strong negative Eu anomaly (Eu/Eu* = 0.20) and the overall depletion in middle REEs (Fig. 14) require significant plagioclase and hornblende crystallization.

In the primitive mantle-normalized multi-element diagram (Fig. 15), the gabbro, monzogabbro, monzonite, and syenites show similar patterns with different abundance levels, suggesting that these rocks may be genetically related. They all have negative Th, Nb and Ta anomalies, and with the exception of syenite, negative Zr and Hf anomalies are also conspicuous. Such trace

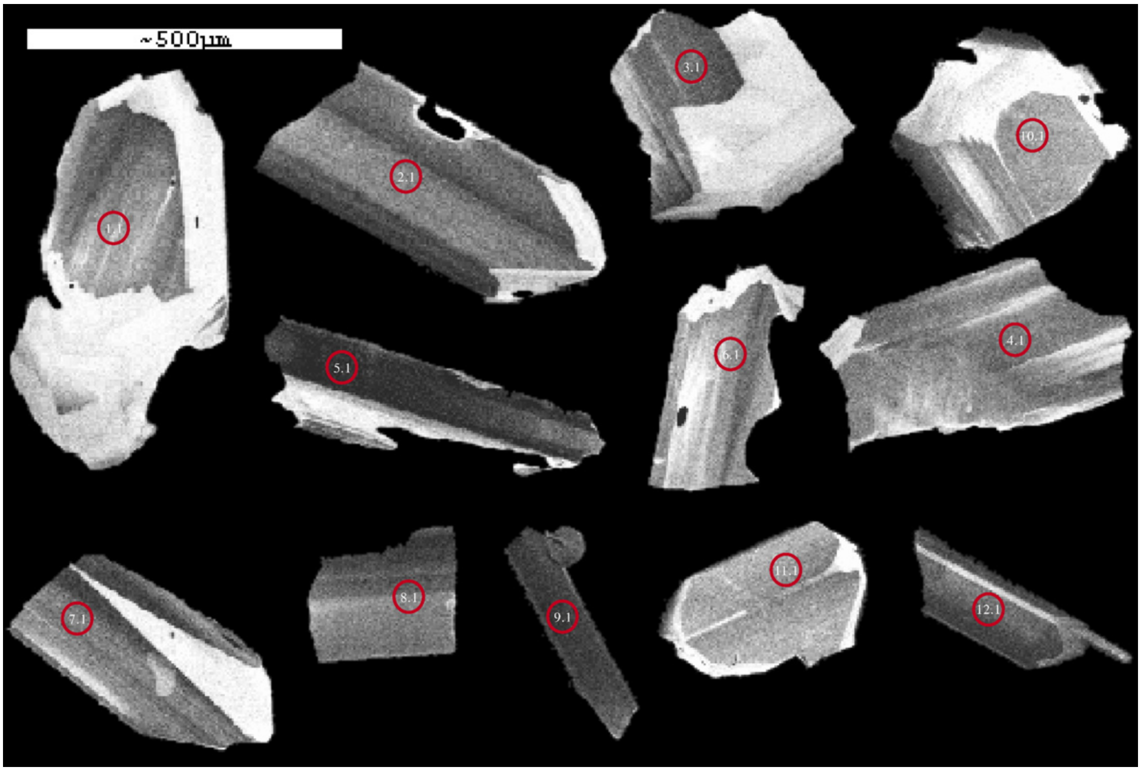

Fig. 6. Cathodoluminescence (CL) images of zircon crystals from monzonite dated by SHRIMP $^{206}Pb/^{238}U$ method at spots circled with labels.

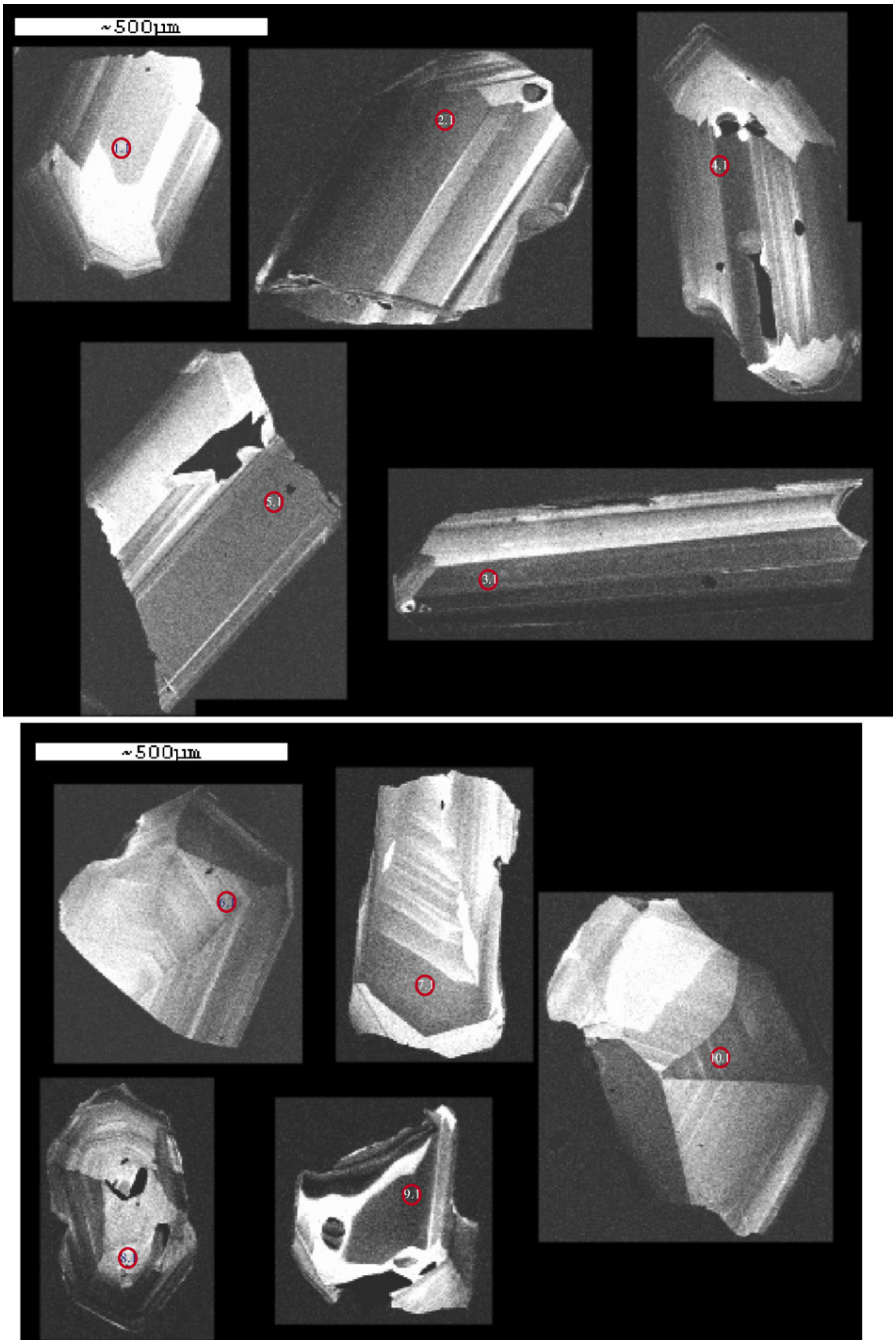

Fig. 8. Cathodoluminescence (CL) images of zircon crystals from syenite dated by SHRIMP $^{206}Pb/^{238}U$ method at spots circled with labels.

element systematics resemble the composition of average continental crust and also are consistent with trace element patterns expected in subduction zone related magmatic rocks. It is possible that these rocks may indeed be genetically associated with subduction zone magmatism, but the relative depletion of Rb with respect to Ba is inconsistent with this interpretation. Also, as gabbros and monzogabbros are dominated by cumulate minerals (Niu et al., 2002), the bulk-rock trace elements are thus largely determined by the type and abundance of mineral phases present instead of melt compositions. The granite differs from the above rocks in

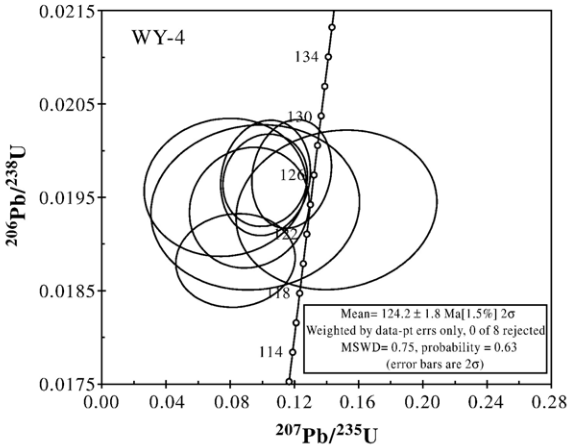

Fig. 9. SHRIMP U–Pb age dates of zircon crystals from syenite as shown in Fig. 8.

having strong negative Ba, Sr, and Ti anomalies, suggesting significant titanomagnetite and plagioclase fractionation during its early magmatic evolution.

4.4. Sr, Nd and Pb isotopes

All the lithologies of the Xuejiashiliang complex have Nd isotope ratios ($^{143}Nd/^{144}Nd$) in the range of 0.51185–0.5120, similar to Mesozoic mafic igneous rocks elsewhere from the North China Craton (Zhou et al., 2001; Li et al., 2001; Hong et al., 2003). The ε_{Nd} value varies from −6.5 to −7.9 for the gabbro, monzogabbro, monzonite, syenite, but −11.3 for the granite. Sr isotope ratios ($^{87}Sr/^{86}Sr$) are in the range of 0.70538–0.70566 for the gabbro, monzogabbro, monzonite and syenite, while the ratio for the granite is 0.89548, significantly higher than in all other rocks. This is largely due to ^{87}Sr ingrowth because of the unusually low Sr and high Rb values (thus the elevated Rb/Sr ratio of ~22.4). Pb isotope ratios $^{206}Pb/^{204}Pb$ (Table 2) for rocks from the Xuejiashiliang complex are in the range of 16.137–16.479, lower than igneous rocks elsewhere from eastern China. Such low $^{206}Pb/^{204}Pb$ ratios are best explained by their source rocks having long term U depletion with low U/Pb ratios. Lower crust with ancient (Proterozoic or earlier) depletion (e.g., ancient granulitic residue of granitic melt extraction) may be the best candidate.

5. Petrogenesis

There are several lines of evidence for the monzonite to result from magma mixing. These include mafic enclaves in the monzonite and the good linear trends among monzogabbro, monzonite, and syenite (see Fig. 13). In Th–Hf/3-Ta diagram, gabbro, monzogabbro, monzonite, syenite, and granite plot along the crust–magma interaction trend (Fig. 16). In Th/Yb–Ta–Yb space (Fig. 17), the petrogenesis of the Xuejiashiliang complex may also be interpreted as a result of mixing between continental crust and mantle derived melts (Fig. 17).

On $^{143}Nd/^{144}Nd$ vs. $^{87}Sr/^{86}Sr$ diagram (Fig. 18), the gabbro, monzogabbro, monzonite, and syenite essentially have the same isotope values and plot in close proximity to the field of enriched mantle EMI component and

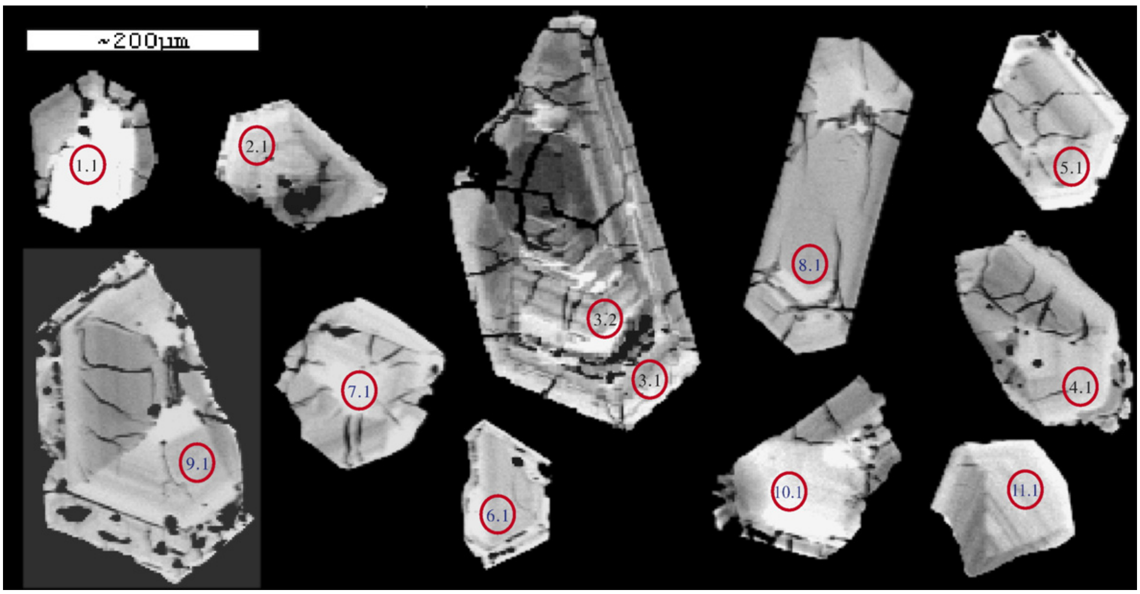

Fig. 10. Cathodoluminescence (CL) images of zircon crystals from granite dated by SHRIMP $^{206}Pb/^{238}U$ method at spots circled with labels.

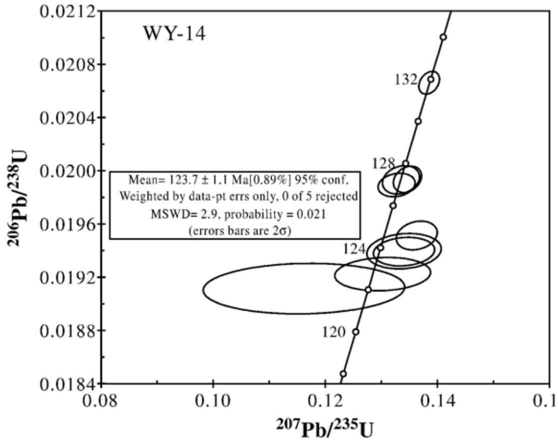

Fig. 11. SHRIMP U–Pb age dates of zircon crystals from granite as shown in Fig. 10.

towards the field defined by lower crust xenoliths (Fig. 18; Deng et al., 2007-this issue). The very high $^{87}Sr/^{86}Sr = 0.89548$ (plotted outside the diagram) of the granite is largely due to radiogenic ingrowth of ^{87}Sr because of very high Rb/Sr ratios (22.4; also see above). Plagioclase fractionation explains the Sr depletion (Fig. 15; also the Eu depletion in Fig. 14), which contributes to the high Rb/Sr ratio of the granite. The high Rb/Sr ratio may also be due to the high Rb content in the granite, probably inherited from its source that is most likely previously highly evolved upper crustal (granitic) material. On $^{143}Nd/^{144}Nd$ vs. $^{206}Pb/^{204}Pb$ diagram (Fig. 19), all the rocks plot in close proximity to the EMI field.

These isotopic characteristics are readily explained by a crust–mantle interaction model (e.g., Voshage et al., 1990; Kempton and Harmon, 1992; Patino Douce and Beard, 1995). That is, the interaction of mantle derived basaltic melts with the Archean lower crust in the North China Craton (NCC) without the need of invoking an EMI-dominated mantle beneath eastern China (e.g. Menzies and Xu, 1998; Griffin et al., 1998; Xu, 2001; Zhou et al., 2002; Chen et al., 2003). In terms of physical processes, we interpret that the Xuejiashiliang complex represents as napshot of crust–mantle interaction. That is, mantle derived basaltic melts underplated beneath or intruded into the deep continental crust. These melts caused deep crustal melting, producing melts with syenitic (high pressure) compositions. Thus, the Xuejiashiliang gabbro, monzogabbro, monzonite, and syenite are intermediate products between the underplated mantle melts and the syenitic melts (also see Fig. 12). Their compositional deviation from simple melting-induced mixing can be better explained as resulting from varying crustal compositions and different differentiation paths of the resulting melts. The granite may have acquired its geochemical characteristics through combined effects of source contribution (e.g., previously highly evolved upper crustal material) and advanced degrees of crystallization-differentiation.

6. On the mantle resource material of Xuejiashiliang complex

Mesozoic gabbro–pyroxenite rocks of the NCC and Dabie orogenic belt share similar geochemical characteristics (Hong et al., 2003). They are rich in light REEs and large ion lithophile elements (LILEs), yet relatively depleted in high strength field elements (HFSEs; e.g., Nb, Ta, Ti), have very low $\varepsilon_{Nd}(t)$ and $^{206}Pb/^{208}Pb$ isotope values, and variable initial $^{87}Sr/^{86}Sr$ ratios. These characteristics have brought about different views on the nature of the Mesozoic basaltic mantle sources. One view is that the gabbro–pyroxenite rocks were derived from partial melting of an enriched mantle with EMI-like geochemical characteristics (Jahn et al., 1999; Zhang et al., 2001a,b; Zhou et al., 2001; Qian et al., 2002; Hong et al., 2003; Yang et al., 2005). Another view is that the mantle source is normal asthenospheric mantle (Deng, 2004). The third view is that the mantle source is a mix between the crustal component of the subducted/subducting south China lithosphere and the "mantle wedge" beneath the NCC (Li et al., 2005).

We know that the Xuejiashiliang gabbro, the most mafic rock type of the complex, cannot represent primary magmas, because they consist of cumulate crystals from a significantly evolved (vs. "primary") mantle melt (see Niu et al., 2002; Niu, 2005a). More over, if we assume that the

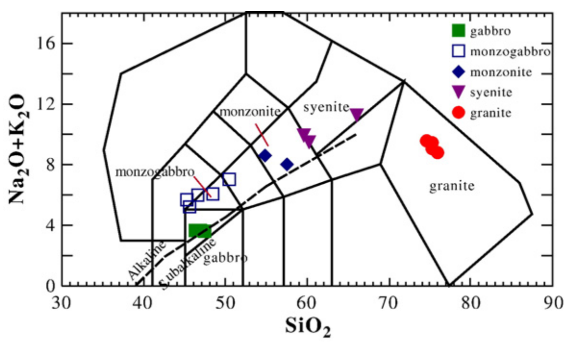

Fig. 12. Total alkali vs. silica (TAS) diagram (after Middlemost, 1994) for samples from the Xuejiashiliang complex. The dash line denotes the division between alkaline and subalkaline rocks following Irvine and Baragar (1971) (other data from Bai et al., 1991; Wang and Zhang, 2001).

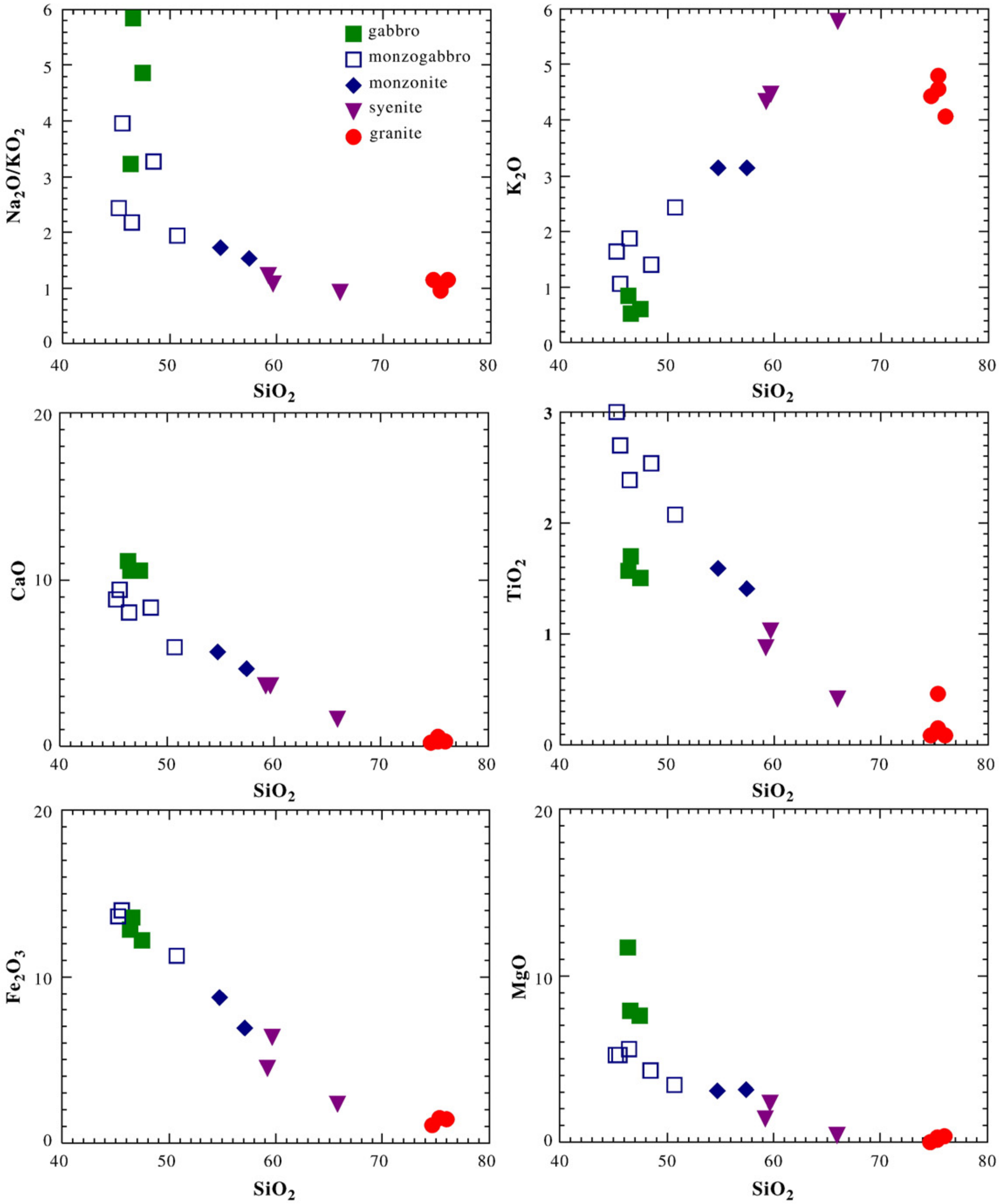

Fig. 13. SiO_2 variation diagrams of abundances and ratios of representative major element oxides for examples from the Xuejiashiliang complex.

bulk-rock trace element contents of the gabbro approximately reflect its parental mantle melt, then such melt differs significantly from the expected EM1 mantle derived melts (Fig. 20). We thus emphasize that the mantle source ultimately responsible for the Xuejiashiliang gabbro is not the postulated EMI-like source, but incompatible element depleted asthenosphere, which is more depleted than EM1 and HIMU sources (see Fig. 20). However, we stress that the EMI-like isotopic signature of the Xuejiashiliang gabbro and other lithologies (Figs. 18, 19) was likely derived from the Archean lower crust, represented by the lower crust xenoliths (Fig. 18) (Deng et al., 2007-this issue). The large negative ε_{Nd} value is not a mantle asthenospheric signature, but was produced by

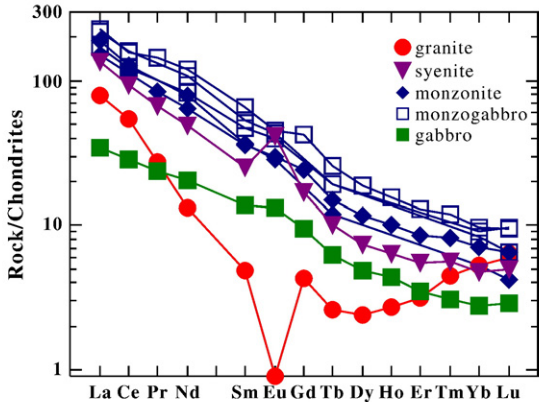

Fig. 14. Chondrite-normalized rare earth element diagrams for samples from the Xuejiashiliang complex.

the mantle melt interaction with the Archean lower crust. This interpretation is consistent with the large scale magmatic activities during the early stage of Early Cretaceous in much of eastern China (Deng et al., 2004).

7. Discussions and conclusions

While the available data do not yet permit definitive conclusions, we can make the following tentative statements, some of which we think are correct, but others need further verification.

(1) The Xuejiashiliang complex represents a snapshot of crust–mantle interaction. Such interaction involves melting of crustal materials induced by mantle derived basaltic melts.
(2) Given the fact that granitoid intrusives are widespread along the Yanshan orogenic belt, we infer that mantle melting and basaltic magmatism must represent a major event. While the nature and origin of this mantle event is debatable (see Niu, 2005a; Deng et al., 2005, 2007-this issue), we stress that this mantle event must have played an important role in the Yanshanian orogenesis.
(3) The Xuejiashiliang gabbro resulted from cooling and differentiation of a mantle derived melt that underplated or intruded the lower crust. The monzogabbro may be the product of deep crustal assimilation of this mantle derived melt. The

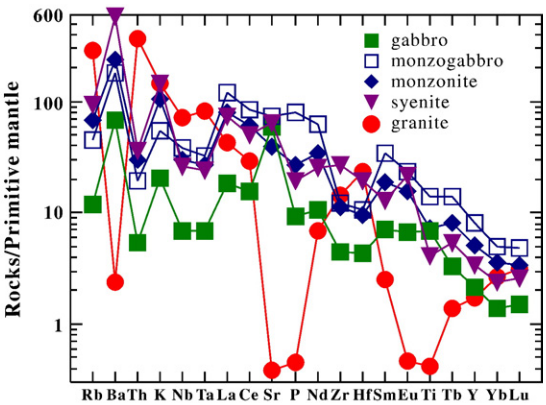

Fig. 15. Primitive mantle-normalized multi-element diagram for samples from the Xuejiashiliang complex. Normalization values from Sun and Mc Donough (1989).

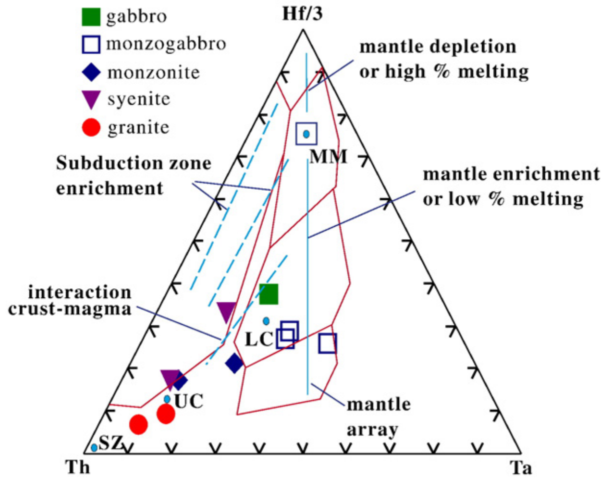

Fig. 16. Th–Hf/3-Ta diagram (Pearce and Peate, 1995) for samples from the Xuejiashiliang complex.

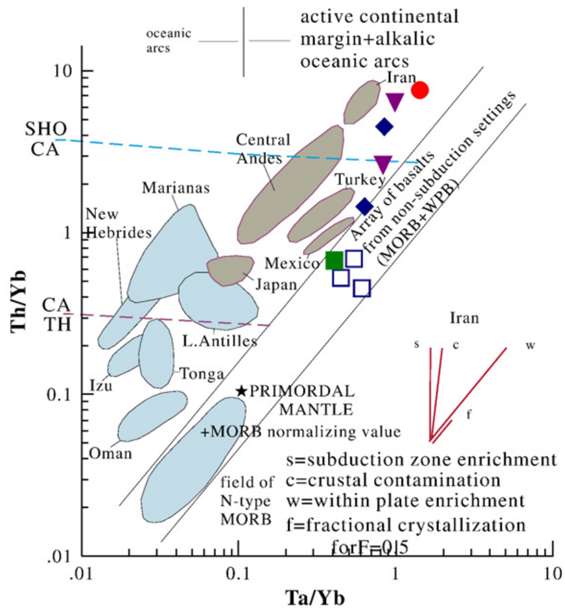

Fig. 17. Th/Yb vs. Ta/Yb diagram (Pearce, 1983) for samples from the Xuejiashiliang complex. Symbols areas in Fig. 16.

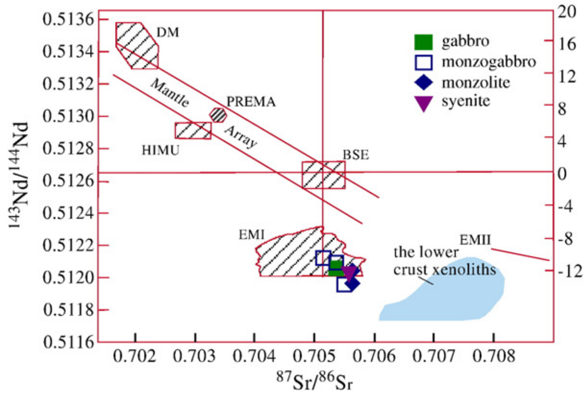

Fig. 18. Nd/^{144}Nd vs. ^{87}Sr/^{86}Sr plot for gabbro, monzogabbro, monzonite and syenite of the Xuejiashiliang complex (after Zindler et al., 1982).

syenite may have solidified from a melt produced by deep crustal melting caused by the mantle derived melt. The monzonite may have formed from mixing of melts parental to the syenite and monzogabbro. In other words, all the diverse lithologies may have resulted from varying degrees of mantle melt induced crustal melting, melt assimilation, differentiation, and mixing.

(4) The Xuejiashiliang granite is best interpreted as upper crustal melt with advanced degrees of differentiation and crystallization of hornblende, alkali-feldspar, plagioclase, and titanomagnetite.

(5) The remarkably similar radiogenic Nb–Sr–Pb isotopes of all these lithologies (except for ^{87}Sr/^{86}Sr of the granite) point to a common source material they share. This common source material with an "EM1-like" isotopic signature could be ancient metasomatized lithospheric mantle or "EM1-like" asthenospheric source. However, if Sr, Nd and Pb abundances in mantle derived melts are less abundant than those in the crust (note that >1000 ppm Sr in the gabbro, monzogabbro and syenite), then mantle isotopic signatures would be overcome by the crustal level processes. The isotopic similarity between these lithologies and the lower crust xenoliths of eastern China (Figs. 18, 19) suggests that the lower crust is isotopically the best candidate for the common source. The elevated ^{87}Sr/^{86}Sr (0.8955) of the granite results from excess radiogenic ingrowths of ^{87}Sr due to elevated Rb/Sr = 22.4, which largely resulted from plagioclase fractionation that depleted Sr (and also Eu; Figs. 14, 15).

(6) The elevated $[La/Yb]_{CN}$ and high Sr/Y ratios of all these lithologies are consistent with the interpreted conditions with garnet as an equilibrium phase (either a residual phase or a liquidus phase). The genesis of melts parental to the syenite requires equilibration pressures equivalent to depth in excess of >50 km (e.g., Wyllie, 1984; Deng et al., 1998). All these suggest persuasively that the melts parental to and the processes responsible for the Xuejiashiliang complex originated and took place at the base of the thickened crust during episodes of compressional tectonism prior to the lithosphere thinning. (Deng et al., 2004, 2007-this issue).

(7) The Xuejiashiliang complex is ~130–123.7 Ma, corresponding to the early stage of Early Cretaceous (K_1^1). If the large scale magmatism reflects the effects

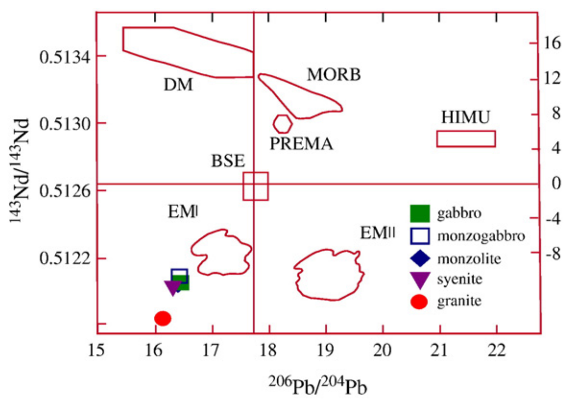

Fig. 19. ^{143}Nd/^{144}Nd vs. ^{206}Pb/^{204}Pb plot for the gabbro, monzogabbro, monzonite and syenite of the Xuejiashiliang complex (after Zindler et al., 1982).

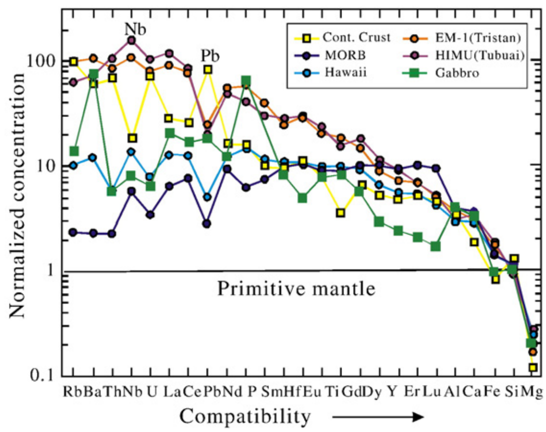

Fig. 20. Comparison of the average Xuejiashiliang gabbro with average mid-ocean ridge basalts (MORB), continental crust, EM-I (from Tristan ocean island), HIMU (from Tunuai island) and Hawaii tholeiite on primitive mantle-normalized multi-element diagram (after Hofmann, 1997).

of lithosphere thinning (Kay and Kay, 1993; Wu et al., 2003; Deng et al., 2004), then the complex would be the consequence of the lithosphere thinning beneath eastern China. The question remains what may have actually caused the lithosphere thinning. Volumetrically significant basaltic magma underplating and eclogitization have been interpreted to raise the bulk density of the lithosphere, thus allowing portions of the lithosphere to founder into the asthenosphere. If this is the immediate mechanism of lithosphere thinning, then the ultimate cause of the lithosphere thinning lies in the origin of volumetrically significant basaltic magmatism beneath eastern China in the Mesozoic.

(8) The lack of evidence for thermal mantle plumes beneath eastern China (Niu, 2005a) rules out mantle plume as a plausible cause of the lithosphere thinning and the coeval magmatism in the Mesozoic. However, the presence of ancient oceanic slabs lying horizontally in the transition-zone beneath eastern China suggests the possibility that the lithosphere thinning may be caused by hydration-weakening at its base with the water, or more likely in the form of hydrous melts, derived from dehydration of the transition-zone oceanic slabs (Niu, 2005a; Niu et al., 2005b). Further efforts are needed to test these hypotheses.

(9) We emphasize that whatever processes may have caused the lithosphere thinning, the key lies in correctly understanding the nature and origin of the mantle event(s) responsible for volumetrically significant basaltic magmatism beneath eastern China in the Mesozoic. We assert that the Yanshanian orogenesis, the coeval lithosphere thinning and large scale granitic magmatism in eastern China, not just NCC, are consequences of the Mesozoic mantle event(s) in the region.

Acknowledgements

This study was supported by the National Natural Science Foundation of China (40234048, 40472051), and the 111 Project from the Ministry of Education and the State Administration of Foreign Experts Affairs (B07011). Y. Niu thanks Durham University for support. We thank P. Jian and D. Y. Liu for assistance with SHRIMP dating, J. X. Zhou and Z. Y. Chen for CL imaging, G. Y. Ji, Q. H. Wang, H. Q. Liu for field assistance. We thank P. R. Castillo and Z.-F. Guo for their critical and constructive comments, and S.-G. Song and R. Koole for their editorial efforts.

References

Bai, Z.M., Xu, S.Z., Ge, S.W., 1991. Badaling Granitic Complex. Geol. Pub. House, Beijing, pp. 1–172 (in Chinese).

Bao, Y.G., Liu, Z.F., Wang, S.F., Huang, L.H., Bai, Z.M., 2001. A Century Geological Research in Beijing Area. Geol. Pub.House, Beijing, pp. 1–274 (in Chinese).

BBG (Beijing Bureau of Geology), 1991. Regional Geology of Beijing Municipality. Geol. Pub. House, Beijing, pp. 1–598 (in Chinese with English abstract).

Chen, B., Jahn, B.M., Zhai, M.G., 2003. Sr–Nd isotopic characteristics of the Mesozoic magmatism in the Taihang–Yanshang orogen, North China Craton, and implications for Archean lithosphere thinning. Journal of the Geological Society (London) 160, 963–970.

Compston, W., Williams, I.S., Kirschvink, J.L., Zhang, Z., Ma, G., 1992. Zircon U–Pb ages for the early Cambrian time-scale. Journal of the Geological Society (London) 149, 171–184.

Davis, G.S., Zheng, Y.D., Wang, C., Darby, B.J., Zhang, C.H., Gehrels, G., 2001. Mesozoic tectonic evolution of the Yanshan fold and thrust belt, with emphasis on Hebei and Liaoning Provinces northern China. GSA Memoir 194, 171–197.

Deng, J.F., Mo, X.X., Zhao, H.L., et al., 1994. Lithosphere root/de-rooting and activation of the East China continent. Geoscience 8 (3), 349–356 (in Chinese, with English abstract).

Deng, J.F, Luo, Z.H., Zhao, H.L., et al., 1998. Trachyte and syenite: petrogenesis constrained by the petrological phase equilibrium. Collected Works of International Symposium on Geological Science Held at Beijing University, Beijing China. Geol. Pub. House, Beijing, pp. 745–757.

Deng, J.F., Su, S.G., Mo, X.X., Zhao, G.C., Xiao, Q.H., Ji, G.Y., Qiu, R.Z., Zhao, H.L., Luo, Z.H., Wang, Y., Liu, C., 2004. The sequence of magmatic–tectonic events and orogenic processes of Yanshan belt, North China. Acta Geologica Sinica 78 (1), 260–266.

Deng, J.F., Zhao, G.C., Su, S.G., et al., 2005. Structure overlap and tectonic setting of Yanshan orogenic belt in Yanshan era. Geotectonica et Metallogenia 29 (2), 159–165 (in Chinese).

Deng, J.F., Su, S.G., Zhao, G.C., et al., 2007. A possible model for the lithospheric thinning of North China Craton: Evidence from the Yanshanian (Jura-Cretaceous) magmatism and tectonism. Lithos 96, 22–35 (this issue). doi:10.1016/j.lithos.2006.09.009.

Gao, S., Rudnick, R.L., Carlson, R.W., McDonough, W.F., Liu, Y.S., 2002. Re–Os evidence for replacement of ancient mantle lithosphere beneath the North China Craton. Earth and Planetary Science Letters 198, 307–322.

Gao, S., Rudnick, R.L., Yuan, H.L., et al., 2004. Recycling lower continental crust in the North China Craton. Nature 432, 892–897.

Griffin, W.L., Zhang, A., O'Reilly, S.Y., Ryan, C.G., 1998. Phanerozoic Evolution of the Lithosphere beneath the Sino-Korean Craton. In: Flower, M.F.J., Chung, S.-L., Lo, C.-H., Lee, T.-Y. (Eds.), Mantle Dynamics and Plate Interactions in East Asia. AGU Geodynamics Series, vol. 27, pp. 107–126.

Hofmann, A.W., 1997. Mantle geochemistry: the message from oceanic volcanism. Nature 485, 219–229.

Hong, D.W., Wang, T., Tong, Y., Wang, X.X., 2003. Mesozoic granitoids from North China block and Qingling–Dabie–Sulu orogenic belt and their deep dynamic process. Earth Science Frontiers 10, 231–256 (in Chinese, with English abstract).

Huang, W.L., Wyllie, P.J., 1981. Phase relationships of s-type granite with H_2O to 35 kbar: muscovite granite from Harnet peak, South Dakota. JGR 86 (B11), 10515–10529.

Irvine, T.N., Baragar, W.R.A., 1971. A guide to the chemical classification of the common volcanic rocks. Canadian Journal of Earth Sciences 8, 523–548.

Jahn, B.M., Wu, F.Y., Lo, C.H., et al., 1999. Crust-mantle interaction induced by deep subduction of the continental crust: geochemical and Sr-Nd isotopic evidence from post-collisional mafic-ultramafic intrusions of the northern Dabie complex, central China. Chemical Geology 157, 119–146.

Jian, P., Liu, D.Y., Sun, X.M., 2003. SHRIMP U–Pb dating of granites for Baimaxueshan and Ludian, northwestern Guizhou province. Acta Geologica Sinica 24 (4), 337–342.

Kay, R.W., Kay, S.M., 1993. Delamination and delamination magmatism. Tectonophysics 219, 177–189.

Kempton, P.D., Harmon, R.S., 1992. Oxygen isotopic evidence for large-scale hybridization of the lower crust during magmatic underplating. Geochimica et Cosmochimica Acta 56, 971–986.

Li, W.P., Lu, F.X., Li, X., 2001. Geochemical features and origin of volcanics of Tiaojishan formation in western Hills of Beijing. Acta Petrologica et Mineralogica 20, 123–133 (in Chinese with English abstract).

Li, S.G., Wang, F., Yang, W., 2005. Contributions of lower crust to the mantle sources of the Mesozoic igneous rocks from the north China craton and Dabie orogen. Abstract for Petrology and Geodynamics, Hangzhou, Zhejiang, pp. 33–34.

Lu, F.X., Zheng, J.P., Li, W.P., et al., 2000. The main evolution pattern of phanerozoic mantle in the eastern China: the "mushroom cloud" model. Earth Science Frontiers 7 (1), 97–107 (in Chinese, with English abstract).

Middlemost, E.A.K., 1994. Naming material in the magma/igneous rock system. Earth-Science Reviews 37, 215–224.

Menzies, M.A., Xu, Y.G., 1998. Geodynamics of the North China Craton. In: Flower, M.F.J., Chung, S.L., Lo, C.H., Lee, L.Y. (Eds.), Mantle Dynamics and Plate Interactions in East Asia. AGU Geodynamics Series, vol. 27, pp. 155–165.

Niu, Y., 2005a. Generation and evolution of basaltic magmas: some basic concepts and a new view on the origin of Mesozoic–Cenozoic basaltic volcanism in Eastern China. Geological Journal of China Universities 11 (1), 9–46.

Niu, Y., Gilmore, T., Mackie, S., Greig, A., Bach, W., 2002. Mineral chemistry, whole-rock compositions and petrogenesis of ODP Leg 176 gabbros: data and discussion. In: Natland, J.H., Dick, H.J.B., Miller, D.J., Von Herzen, R.P. (Eds.), Proc. ODP, Sci. Results, vol. 176, pp. 1–60.

Niu, Y., Song, S.G., Zhang, L.F., 2005a. The origin, evolution and present state of subcontinental lithosphere — an IUGS-SECE conference report. Episodes 28, 209.

Niu, Y., Song, S.G., Zhang, L.F., Deng, J.F., Mo, X.X., et al., 2005b. Slab dehydration, subcontinental lithosphere thinning and Mesozoic/Cenozoic volcanism in eastern China: a special consequence of plate tectonics. Abstract for the Origin, Evolution and Present State of Subcontinental Lithosphere IUGS-SECE Conference, Beijing, pp. 26–29.

Nutman, A.P., Green, D.H., Cook, C.A., et al., 2001. SHRIMP U–Pb zircon dating of the exhumation of the Lizard peridotite and its emplacement over crustal rocks: constraints for tectonic models. Journal of the Geological Society (London) 158, 809–820.

Patino Douce, A.E., Beard, J.S., 1995. Dehydration-melting of biotite gneiss and quartz amphibolite from 3 to 15 kbar. Journal of Petrology 36, 707–738.

Pearce, J.A., 1983. Role of the sub-continental lithosphere in magma genesis at active continental margins. In: Hawkesworth, C.J., Norry, M.J. (Eds.), Continental Basalt and Mantle Xenoliths. Nantwich, UK, Shiva, pp. 230–249.

Pearce, J.A., Peate, D.W., 1995. Tectonic implications of the composition of Volcanic Arc magmas. Ann. Rev. Earth Planet. Sci. 23, 251–285.

Qian, Q., Chung, S.L., Lee, T.Y., Wen, D.J., 2002. Geochemical characteristics and petrogenesis of the Badaling high Ba–Sr granitoids: a comparison of igneous rocks from North China and the Cabie-Sulu orogen. Acta Petrologica Sinica 18, 275–292 (in Chinese with English abstract).

Rudnick, R.L., Gao, S., Ling, W.L., Liu, Y.S., McDonough, W.F., 2004. Petrology and geochemistry of spinel peridotite xenoliths from Hannuoba and Qixia, North China craton. Lithos 77, 609–637.

Sun, S.S., Mc Donough, W.F., 1989. Chemical and isotopic systematics of oceanic basalts: implications for mantle composition and processes. In: Saunders, A.D., Morry, M.J. (Eds.), Magmatism in the Ocean Basins. Geological Society, London, Special Publications, vol. 42, pp. 313–345.

Voshage, H., Hofmann, A.W., Mazzucchelli, M., Rivalenti, G., Sinigoi, S., Raczek, L., Demarchi, G., 1990. Isotopic evidence from the Ivrea zone for a hybrid lower crust formed by magmatic underplating. Nature 347, 731–736.

Wang, Y., Zhang, Q., 2001. A granitoical complex from Badaling area, North China: composition, geochemical characteristics and its implications. Acta Petrologica Sinica 17, 533–540 (in Chinese with English abstract).

Williams, I.S., 1998. U–Th–Pb geochronology by ion microprobe. Reviews in Economic Geology 7, 1–35.

Wu, F.Y., Ge, W.C., Sun, D.Y., Guo, C.L., 2003. Discussions on the lithospheric thinning in Eastern China. Earth Science Frontiers 10, 51–60 (in Chinese with English abstract).

Wu, F.Y., Ge, W.C., Sun, D.Y., et al., 2002. Discussions on the lithospheric thinning in eastern China. Earth Science Frontiers 10 (3), 51–60 (in Chinese, with English abstract).

Wu, F.Y., Yang, J.H., Wilde, S.A., et al., 2005a. Geochronology, petrogenesis and tectonic implications of Jurassic granites in the Liaodong Peninsula, NE China. Chemical Geology 221, 127–156.

Wu, F.Y., Yang, J.H., Wilde Simon, A., Zhang, X.O., 2005b. Geochronology, petrogenesis and tectonic implications of Jurassic granites in the Liaodong Peninsula, NE China. Chemical Geology 221, 127–156.

Wyllie, P.J., 1984. Constraints imposed by experimental petrology on possible and impossible magma sources and products. Philosophical Transactions of the Royal Society of London. A 310, 439–456.

Xu, Y.G., 2001. Thermal-tectonic destruction of the Archean lithospheric keel beneath the Sino-Korean Craton in China: evidence, timing and mechanism. Physics and Chemistry of the Earth. Part A: Solid Earth and Geodesy 26, 747–757.

Yang, J.H., Wu, F.Y., Chung, S.L., et al., 2005. Petrogenesis of Early Cretaceous intrusions in the Sulu ultrahigh-pressure orogenic belt, east China and their relationship to lithospheric thinning. Chemical Geology 222, 200–231.

Yu, J.H., Zhang, F.L., Fu, H.Q., et al., 1994. Pluton in Beijing. Beijing, Geological Publishing House, pp. 1–196 (in Chinese).

Zhang, Q., Wang, Y., Qian, Q., Yang, J.H., Wang, Y.L., Zhao, T.P., Guo, H., 2001a. The characteristics and tectono-metallogenic significances of the adakites in Yanshan period from East China. Acta Petrologica Sinica 17, 236–244 (in Chinese with English abstract).

Zhang, Q., Qian, Q., Wang, E., Zhao, T., Hao, J., Guo, G., 2001b. An East China plateau in mid-late Yanshanian period: implication from adakites. Scientia Geologica Sinica 36, 248–255 (in Chinese with English abstract).

Zheng, J.P., Sun, M., Lu, F.X., et al., 2003. Mesozoic lower crust xenoliths and their significance in lithospheric evolution beneath the Sino-Korean Craton. Tectonophys 361, 37–60.

Zhou, X.H., Zhang, G.H., Yang, J.H., 2001. Sr–Nd isotope mapping of Late Mesozoic volcanic rocks a cross northern margin of North China Craton and implications to geodynamic processes. Geochimica 30, 10–23 (in Chinese with English abstract).

Zhou, X.H, Sun, M., Zhang, G.H., 2002. Continental crust and lithospheric mantle interaction beneath North China: isotopic evidence from granulite xenoliths in Hannuoba, Sino-Korean craton. Lithos 62, 111–124.

Zindler, A., Jagoutz, E., Goldstein, S., 1982. Nd, Sr and Pb isotopic systematics in a three-component mantle: a new perspective. Nature 298, 519–523.